

# Development of Bio-based Membranes for Building Envelope Applications from Poly(lactic acid) and Cellulose Microfibers

Masoud Dadras Chomachayi,<sup>a,\*</sup> Pierre Blanchet,<sup>a</sup> and Atif Hussain<sup>b</sup>

A bio-based membrane was developed for building envelope applications. Biocomposites with enhanced water vapor permeability were fabricated based on poly(lactic acid) (PLA) and cellulose microfibers (CMF). To improve the interfacial adhesion between PLA and fibers, polyethylene glycol (PEG) was used as a compatibilizer for the modification of CMF. The properties of prepared PLA-based biocomposites were investigated in terms of their morphology, thermal stability, thermomechanical properties, and water vapor permeability. The morphological investigation showed the improved dispersion of cellulose fibers in the PLA matrix after modification of the bio-filler with PEG. The thermogravimetric analysis illustrated that the addition of modified CMFs increased the thermal stability of materials. Moreover, the water vapor permeability of PLA-based biocomposites was enhanced by adding modified CMFs to the PLA matrix. The results suggest that the utilization of PEG as a biopolymer compatibilizer represents a cost-effective and environmentally friendly method to improve the properties of PLA/CMF biocomposites. The developed membranes are potential materials for the fabrication of bio-based membranes with permeable properties that facilitate the transmission of entrapped water vapor through the building, eventually prolonging the service life of building envelope materials.

DOI: 10.15376/biores.17.4.5707-5727

Keywords: Poly(lactic acid); Cellulose microfibers; Modification; Bio-based materials; Building envelope

Contact information: a: Department of Wood and Forest Sciences, Laval University, Québec City, QC, Canada; b: Department of Materials Engineering, University of British Columbia, Vancouver, BC, Canada; \*Corresponding author: masoud.dadras-chomachayi.1@ulaval.ca

## INTRODUCTION

The International Energy Agency reported that buildings are responsible for considerable global energy consumption (~40%) and CO<sub>2</sub> emissions. Sustainable building construction designs use innovative systems to reduce energy consumption and positively impact the natural environment (Arregi *et al.* 2020). The building envelope is the main part of buildings responsible for protecting the interior atmosphere from external environmental impacts such as wind, rain, industrial pollution, and acoustic effects. The most important functions of the building envelope are water vapor permeability, air leakage, water resistance, heat transfer resistance, thermal and mechanical stability, flammability and acoustic properties (Iwaro and Mwashia 2013). There are several types of envelope systems used in building construction, but there are many problems associated with conventional envelopes. For instance, common façade systems such as aluminum, concrete, and oil-based materials are responsible for about 23% of global CO<sub>2</sub> emissions (Gustavsson and

Sathre 2006). The increasing production trend of conventional polymers, which are generally made of heavy crude oil, is related to fossil resource depletion and negatively affects the environment (Abdul-Latif *et al.* 2020).

Biopolymers are synthesized by polymerizing bio-based monomers or by extracting polymers from biomass and biomaterials produced in microorganisms. Poly(lactic acid) (PLA), polycaprolactone (PCL), and polyhydroxyalkanoate (PHA) are examples of biopolymers used in plastic applications industry (Astudillo *et al.* 2018). While these polymers have some disadvantages that restrict their applications, employing additives or combining them with other materials improves their properties. Wood-plastic composite (WPC), which is a polymer matrix incorporated with wood, cellulose, or other natural fibers, has become popular in several applications due to its attractive performance and sustainability (Eder and Carus 2013). In WPC materials, the polymeric matrix defines the shape of composites, transfers the load to reinforcements, and provides the required properties in the considered application. The reinforcements (plant/natural fibers) provide strength, stiffness, and hygroscopicity to materials (Siró and Plackett 2010).

PLA is the most interesting biopolymer used in the plastic industry. It is produced from the ring-opening polymerization of lactide monomers extracted from renewable resources. PLA has several potential advantages, including excellent processability, thermal plasticity, and proper optical and mechanical properties (Chomachayi *et al.* 2020). Cellulose microfibril (CMF) is derived from cellulose from plants. Some advantages of CMF are its abundance, high mechanical strength, low cost, and renewability, which make it an ideal candidate for reinforcing polymer composites (Bledzki and Gassan 1999). CMF tends to aggregate when introduced within non-polar polymers such as PLA, which limits the reinforcing effects of the bio-filler (Fortunati *et al.* 2013; Lu *et al.* 2014; Mármol *et al.* 2020). The agglomeration of fibers is due to their highly hydrophilic behavior, the strong hydrogen bonding between the hydroxyl groups of cellulose, and poor fiber-polymer matrix interfacial adhesion (Singh *et al.* 2020). Hence, CMF should be modified to improve the properties of composites.

There are various ways to modify CMF. For instance, Hussain and Blanchet (2021) studied the effect of an organic surfactant (Shwago-wett 6267) on the properties of PLA/CMF composites. The treated fibers showed improved dispersibility in the PLA matrix. Moreover, the treatment enhanced the thermal properties of materials, including the glass transition temperature and thermal degradation temperature, as well as the water-resistance properties. Moreover, Johari *et al.* (2016) used maleic anhydride (MA) to increase the intermolecular interaction between PLA and CMF. The morphology results indicated that adding 5 wt% of MA remarkably improved the dispersion of fibers in the PLA matrix. Additionally, the values of tensile strength and modulus of materials were enhanced due to the reinforcing effect of the treated fibers. Singh *et al.* (2020) modified CMF with poly(ethylene oxide) (PEO) and investigated the properties of PLA-based composites. The results revealed that PEO acted as compatibilizer and plasticizer in composites, improving the interfacial adhesion between the PLA matrix and fibers. Furthermore, the modification with PEO increased the dispersion of CMF bio-filler in the PLA matrix and improved the mechanical properties of materials. Moreover, it was found that PEO can be used to promote the dispersion of graphene nanoplatelets (GNP) in the PLA matrix and resulted in improvement of the mechanical properties and crystallization ability of PLA/GNPs nanocomposites (Zeng *et al.* 2019). Similarly, Ye *et al.* (2019) investigated that the addition of modified GNP with PEO significantly improved the

toughness and thermal stability of PLA/poly(butylene adipate-co-terephthalate) (PBAT) blends.

The objective of this study was to develop bio-based biocomposites to serve as membranes with enhanced permeability properties for building envelope applications. In this regard, biocomposites were fabricated from PLA biopolymer and commercially available cellulose fibers. To improve the compatibility and interfacial adhesion between fibers and PLA, PEG was grafted onto the surface of CMF using 1,1'-carbonyldiimidazole coupling agent. The PLA-based biocomposites were investigated in terms of their morphology, water vapor permeability, and thermal and mechanical characteristics.

## EXPERIMENTAL

### Materials

Commercial grade PLA (4043D) was purchased from NatureWorks (Minnetonka, MN, USA) and has a melt flow rate of 6 g/10 min (at 210 °C, 2.16 kg). This grade of PLA was used for the fabrication of polymer membranes. Poly(ethylene glycol) (PEG) with an average molecular weight of 8000 gr/mol was supplied by Sigma-Aldrich (Oakville, ON, Canada). Cellulose microfibrils (CMF) produced from northern bleached softwood kraft (NBSK) pulp containing 1 wt% water with an average diameter of  $8 \pm 1 \mu\text{m}$ , and a bulk density of 633 kg/m<sup>3</sup> (moist fluff) was provided from the Kruger Biomaterials Inc. (Montreal, Quebec, Canada). Dimethyl sulfoxide (DMSO), chloroform, 1,1'-carbonyldiimidazole (CDI), and methanol were also purchased from Sigma-Aldrich (Oakville, ON, Canada).

### Modification of Cellulose Microfibrils

#### *Mixing of CMF with PEG*

In order to modify CMF, 20 g of PEG was dissolved in 400 mL of distilled water (5 wt%) by continuously stirring at 500 rpm for 3 h at 40 °C to yield transparent viscous solutions. Then, 10 g of CMF was mixed with the PEG solution (ratio of CMF:PEG was 1:2) under stirring at 500 rpm for 24 h at 40 °C. The resulting solution was freeze-dried for two days and then ground to obtain CMF-PEG powder.

#### *Grafting PEG onto CMF*

The PEG-grafted CMF (CMF-G-PEG) was prepared in a two-step process. First, 10 g of CMF and CDI (1:1 ratio) were suspended in 250 mL of DMSO and allowed to react at 40 °C for 2.5 h while being stirred at 500 rpm. The resultant suspension was centrifuged twice at 5000 rpm for 45 min to remove the unreacted CDI traces. In the second step, 20 g of PEG was added to 400 mL of DMSO and mixed with the CDI-activated CMF under stirring at 500 rpm for 24 h at 40 °C. The prepared suspension was centrifuged twice at 5000 rpm for 45 min to remove the unreacted PEG. The precipitate was washed with hot methanol and centrifuged at 5000 rpm for 30 min, and subsequently dried in a vacuum oven for 2 days at 70 °C. Finally, the dried CMF-G-PEG was ground to obtain a powder. The final weight of modified CMF was 12.7 g, showing a net gain of 2.7 g in grafted PEG. The modification of CMF is illustrated in Fig. 1.

## Preparation of PLA-based Biocomposites

The polymer biocomposites were prepared through the solvent casting method. Firstly, 5 g of PLA was dissolved into 100 mL of chloroform under stirring at 600 rpm for 3 h at room temperature. The PLA solution was then mixed with different amounts of untreated and modified CMFs and stirred for 30 min using a high shear mixer at 1200 rpm. The prepared solutions were poured into a glass Petri dish, and the solvent was evaporated at room temperature in a fume hood. Before characterization, the biocomposite films were dried in a vacuum oven overnight at 80 °C to evaporate any remaining solvent. The biocomposites formulation is given in Table 1.

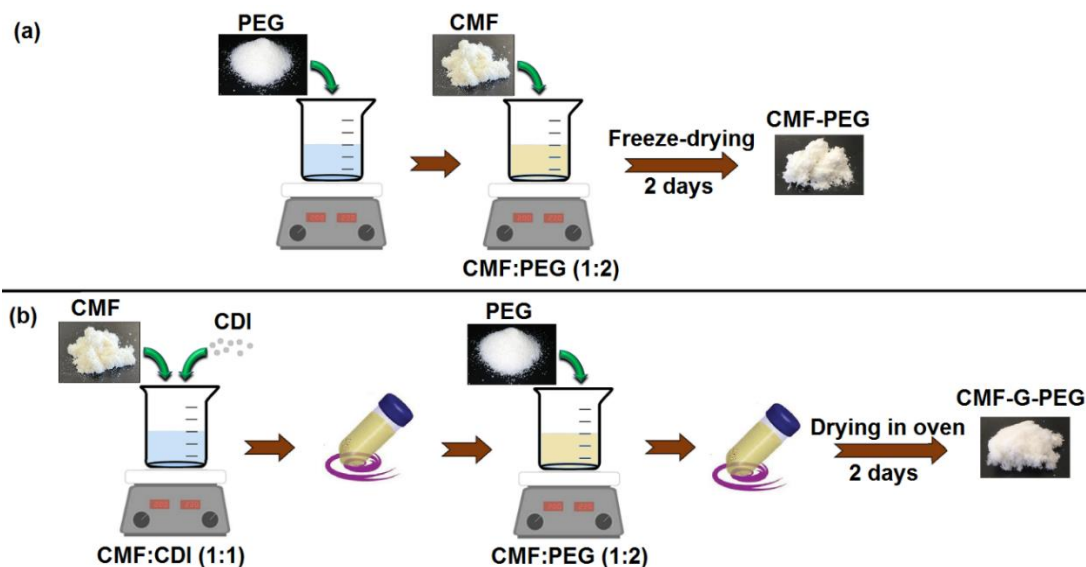


Fig. 1. Modification procedures of CMF: (a) mixing of CMF with PEG; (b) grafting PEG onto CMF

Table 1. PLA-based Biocomposites Formulation

Material	PLA (wt%)	CMF (wt%)	CMF-PEG (wt%)	CMF-G-PEG (wt%)
PLA	100	-	-	-
PLA/C5	95	5	-	-
PLA/C10	90	10	-	-
PLA/C15	85	15	-	-
PLA/C20	80	20	-	-
PLA/C25	75	25	-	-
PLA/C30	70	30	-	-
PLA/CP5	95	-	5	-
PLA/CP10	90	-	10	-
PLA/CP15	85	-	15	-
PLA/CP20	80	-	20	-
PLA/CP25	75	-	25	-
PLA/CP30	70	-	30	-
PLA/CGP5	95	-	-	5
PLA/CGP10	90	-	-	10
PLA/CGP15	85	-	-	15
PLA/CGP20	80	-	-	20
PLA/CGP25	75	-	-	25
PLA/CGP30	70	-	-	30

## Characterization Techniques

### *Scanning electron microscope (SEM)*

The morphology study of cellulose microfibrils and PLA-based biocomposites was carried out using a JEOL 6360LV SEM (Hitachi, Japan) operated under vacuum conditions. The accelerating voltage was set at 15 kV. Before the observation, the surfaces of samples were coated with a thin layer of pure gold by an EMS 950x sputter coater.

### *Fourier-transform infrared spectroscopy (FT-IR)*

Fourier-transform infrared spectroscopy (FT-IR) was used to obtain an infrared absorption spectrum of untreated and modified CMF and PLA-based biocomposites. The infrared spectra of samples were recorded using an INVENIO® R (Bruker, Karlsruhe, Germany). The scans were collected in absorbance mode from 4000 to 400  $\text{cm}^{-1}$  at 4  $\text{cm}^{-1}$  resolutions.

### *Thermogravimetric analysis (TGA)*

Thermogravimetric analysis was used to examine the thermal degradation behavior of materials. The TGA was performed using a TGA/DTA 851e Mettler Toledo instrument (Columbus, OH, USA). The TGA test was conducted under a nitrogen atmosphere purged at 50 mL/min. Cellulose microfibrils and PLA-based biocomposites were respectively heated from 25 to 900 °C and 25 to 600 °C at a heating rate of 10 °C/min.

### *Differential scanning calorimetry (DSC)*

Differential scanning calorimetry was used to determine the glass transition temperature ( $T_g$ ) and melting temperature ( $T_m$ ) of materials using a DSC Mettler Toledo 822/e (Columbus, OH, USA). The measurements were carried out at different temperatures: 25 to 400 °C (for untreated and modified CMF) and 25 to 250 °C (for PLA-based biocomposites) at 10 °C/min under a nitrogen atmosphere purged at 50 mL/min.

### *Dynamic mechanical analysis (DMA)*

Dynamic mechanical analysis was conducted to study the effect of different cellulose microfibrils on the values of storage modulus ( $E'$ ) and glass transition temperature ( $T_g$ ) of the materials. The DMA experiment was performed using a Q800 dynamic mechanical analyzer (TA Instruments, New Castle, DE, USA) in tension mode at the frequency and amplitude of 1 Hz and 10  $\mu\text{m}$ , respectively. Each specimen was cut using a laser machine into a rectangular shape with a dimension of 2 cm  $\times$  0.45 cm with an approximate thickness of  $\sim$ 300  $\mu\text{m}$ . The test was performed from 30 to 100 °C at a heating rate of 3 °C/min.

### *Tensile test*

The mechanical performance of PLA-based biocomposites was studied using a uniaxial tensile testing machine according to the ASTM D882-10 standard (2010). The tensile test was performed with a load cell of 500 N at a crosshead speed of 12.5 mm/min. Each specimen was cut using a laser machine into a rectangular shape with a dimension of 10 cm  $\times$  1 cm with an approximate thickness of  $\sim$ 300  $\mu\text{m}$ . The Young's modulus (MPa), tensile strength (MPa), and elongation at break (%) of samples were calculated from the stress-strain curves. Three replications were considered for each specimen ( $n=3$ ), and the average values were reported.

*Water vapor transmission rate (WVTR)*

The water vapor transmission rate (WVTR) of biocomposites was characterized according to ASTM E96/E96M-16 (Method B) (2016). Films of the materials with an approximate thickness of 300  $\mu\text{m}$  were cut circular and mounted on the mouth of a permeability cup with an internal diameter of 6 cm containing 170 mL of distilled water and then weighed ( $W_0$ ). The surrounding film's area was sealed with silicone sealant to avoid water vapor loss through the boundaries. The cups were placed in a conditioning chamber at  $23 \pm 1$  °C and relative humidity (RH) of  $50 \pm 1\%$ . The weights of cups were measured every day for two weeks ( $W_n$ ), and a graph of evaporated water ( $W_0 - W_n$ ) versus time was plotted. The WVTR value was calculated using Eq. 1,

$$WVTR = \frac{(G/t)}{A} (g \cdot h^{-1} \cdot m^{-2}) \quad (1)$$

where  $G$  is the steady-state weight change (g),  $t$  is time (h), and  $A$  is the cup mouth area ( $0.00255 \text{ m}^2$ ). Three replications were considered for each specimen ( $n=3$ ), and the average values of WVTR were reported.

To compare the WVTR values of materials with different thicknesses, the normalized WVTR value was described by eliminating the thickness factor as follows,

$$\text{Normalized WVTR} = WVTR \times d (g \cdot h^{-1} \cdot m^{-1}) \quad (2)$$

where  $d$  is the thickness of materials' film (m).

Moreover, the value of water vapor permeability ( $P$ ) was calculated by Eq. 3,

$$P = \frac{\text{Normalized WVTR}}{\Delta P} = \frac{WVTR \times d}{S \times (R_2 - R_1)} (g \cdot h^{-1} \cdot m^{-1} \cdot Pa^{-1}) \quad (3)$$

where  $S$  is saturation vapor pressure at 23 °C (2,812 Pa) and  $R_1$  and  $R_2$  are the relative humidity of cup (100% RH) and chamber (50% RH), respectively.

## RESULTS AND DISCUSSION

### Characterization of CMF

The morphology of untreated and modified CMFs was studied by SEM, and the results are presented in Figs. 2a-c. The untreated CMF (Fig. 2a) displayed a network of intertwined microfibers with an average diameter of about  $8 \pm 1 \mu\text{m}$ . Figures 2b and 2c show that the morphology of cellulose fibers became more uniform and defined after the modification with PEG. Specifically, in the case of CMF-G-PEG, PEG is uniformly coated around each individual cellulose fiber, resulting in reduced entanglements among fibers. There was no significant change in the diameter of fibers after treatment.

The chemical structure of CMF before and after the modification was analyzed by FT-IR spectroscopy, as presented in Fig. 2d. The untreated CMF exhibited O-H and C-H stretching bands at 3500 to 3000  $\text{cm}^{-1}$  (centered at 3320  $\text{cm}^{-1}$ ) and 2888  $\text{cm}^{-1}$ , respectively. The band at 1157  $\text{cm}^{-1}$  is attributed to the asymmetric ring-breathing vibration of cellulose. The absorption bands at 1090 and 1028  $\text{cm}^{-1}$  are assigned to C-OH stretching of secondary and primary alcohols of cellulose, respectively (Singh *et al.* 2020). In the FT-IR spectrum of PEG, the sharp absorption bands at 2873, 1716, and 1093  $\text{cm}^{-1}$  are attributed to the stretching vibrations of C-H, C=O, and C-O-C, respectively. PEG showed the absorption

bands at 1461 and 1357  $\text{cm}^{-1}$  assigned to the C-H bending vibrations, and a broad peak centered at 3471  $\text{cm}^{-1}$  corresponded to the terminal O-H groups (Charmi *et al.* 2019).

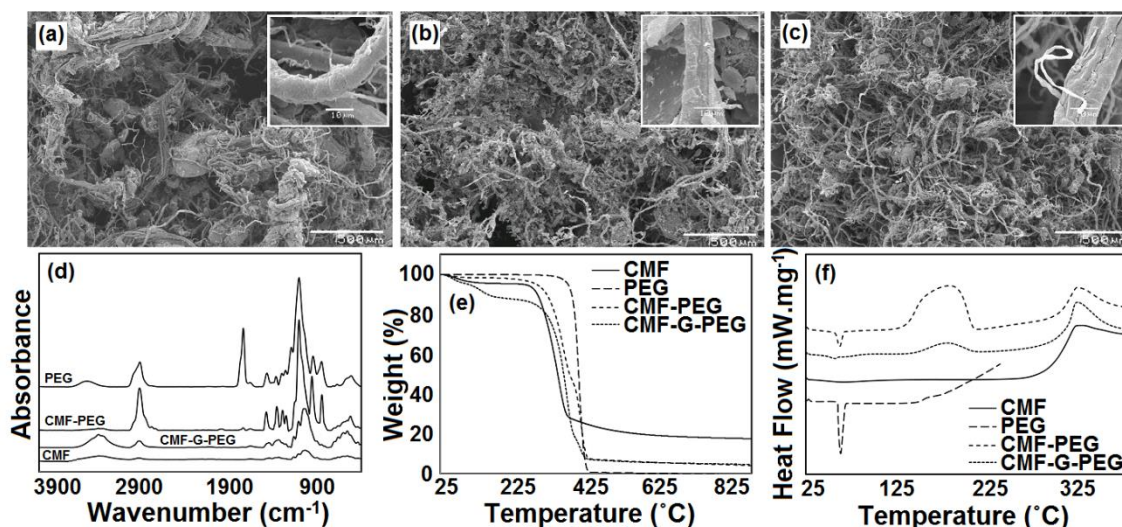


**Fig. 2.** SEM images of: (a) untreated CMF, (b) CMF-PEG, and (c) CMF-G-PEG, (d) FT-IR spectra, (e) TGA, and (f) DSC curves of untreated and modified CMF

It can be observed in the FT-IR spectrum of CMF-PEG that the absorption intensity of C=O and O-H groups of PEG decreased; additionally, the stretching vibrations of C-H and C-O-C groups became more prominent. The results might be attributed to the chemical interactions between hydroxyl groups of CMF and the ether and hydroxyl terminal groups of PEG (Singh *et al.* 2020; Yazdani *et al.* 2021). In the FT-IR spectrum of CMF-G-PEG, the strong stretching vibrations of O-H and C-H bands were observed at 3336 and 2883  $\text{cm}^{-1}$ , respectively. Moreover, the intensity of C-H bending vibrations of PEG increased and shifted to the lower wavenumbers (1424 and 1324  $\text{cm}^{-1}$ ). This could be due to the successful chemical reaction of CMF and PEG. A previous study by Karimi *et al.* (2019) has also reported that PEG was successfully grafted on the surface of graphene oxide nanoparticles thanks to the presence of the CDI coupling agent. As shown in the schematic image (Fig. 3), the nitrogen bonding (R-N=C) in CDI can provide a crucial linkage between the primary and secondary alcohol groups of CMF and the ether or terminal hydroxyl groups of PEG (Lanzilotto *et al.* 2015; Karimi *et al.* 2019).

The TGA results of PEG, untreated, and modified CMFs are presented in Fig. 2e and Table 2. PEG was thermally degraded in a single step in the range of 380 to 420  $^{\circ}\text{C}$ . The temperature for 95% weight loss ( $T_{95}$ ) of PEG is 433.1  $^{\circ}\text{C}$ . In the first decomposition region below 200  $^{\circ}\text{C}$ , the mass of untreated and modified CMFs was decreased slightly due to the removal of moisture. The degradation of untreated CMF occurred in the range of 320 to 400  $^{\circ}\text{C}$ . The CMF-PEG showed a higher value of onset degradation temperature ( $T_{10}$ ) compared to untreated fibers. Moreover, the maximum-rate degradation temperature ( $T_{\text{max}}$ ) of CMF (349.1  $^{\circ}\text{C}$ ) shifted towards higher temperatures after the modification with PEG. The  $T_{\text{max}}$  values of CMF-PEG and CMF-G-PEG were 378.6 and 368.6  $^{\circ}\text{C}$ , respectively. The results confirm that the addition of PEG improved the thermal stability of cellulose fibers.

The first heating DSC thermograms of PEG, untreated, and modified CMFs are given in Fig. 2f. PEG showed a sharp endothermic peak at 65.6 °C, representing its melting temperature ( $T_m$ ). The untreated CMF exhibited an exothermic peak centered at 340.0 °C ( $T_d$ ) with an enthalpy value of 1162 J/g, indicating the thermal decomposition of cellulose fibers. In this range of temperature, the breakage of glycosidic bonds reduces the polymerization degree of cellulose, leading to the formation of hydrocarbon derivatives, CO<sub>2</sub>, and H<sub>2</sub>O. After treatment,  $T_d$  of CMF slightly increased to higher values of 341.8 and 341.6 °C in CMF-PEG and CMF-G-PEG, respectively, indicating the improvement of thermal stability of fibers. This observation verifies the TGA results. Similarly, Lima *et al.* (2018) reported that cellulose nanostructures displayed a considerable increase in thermal stability after the modification with PEG.

**Table 2.** Thermal Parameters of Untreated and Modified CMFs from TGA and DSC Analyses

Material	$T_{10}$ (°C)	$T_{max}$ (°C)	$T_{95}$ (°C)	$T_m$ (PEG) (°C)	$\Delta H_m$ (PEG) (J.g <sup>-1</sup> )	$T_d$ (CMF) (°C)	$\Delta H_d$ (CMF) (J.g <sup>-1</sup> )
CMF	297.84	349.12	-	-	-	340.05	1162.00
PEG	393.69	412.18	433.06	65.55	185.32	-	-
CMF-PEG	323.94	378.62	729.07	64.49	69.54	341.79	800.38
CMF-G-PEG	156.92	368.55	773.47	58.56	14.17	341.59	1014.60

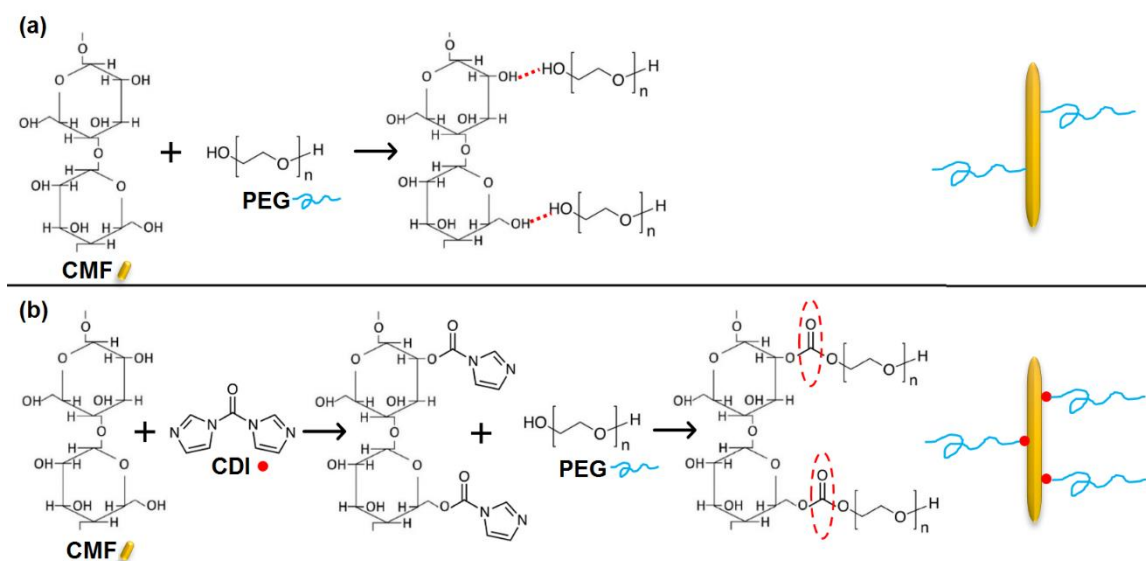


**Fig. 3.** Illustration of surface modification reactions of: (a) CMF with PEG and (b) PEG-grafted CMF

### Characterization of PLA-based Biocomposites

The images of all PLA-based biocomposites are provided in Fig. 4. In order to study the dispersion of untreated and modified CMFs in the PLA matrix, SEM images were obtained from the top surface and fractured cross-sections of materials, and the results are provided in Fig. 5. As shown in Figs. 5a-c, the neat PLA exhibited a smooth morphology without any defects or irregularities, indicating the brittle nature of PLA. In Figs. 5d-f, the morphology images of PLA/C10 (PLA incorporated with 10 wt% of untreated CMF)

indicate the poor dispersion of CMF in the PLA matrix, and fibers were agglomerated at the surface of composites. It might be due to the poor intermolecular interaction between PLA and untreated CMF. Previous studies also reported the agglomeration of cellulose fibers in the PLA matrix (Fortunati *et al.* 2013; Lu *et al.* 2014; Mármol *et al.* 2020).

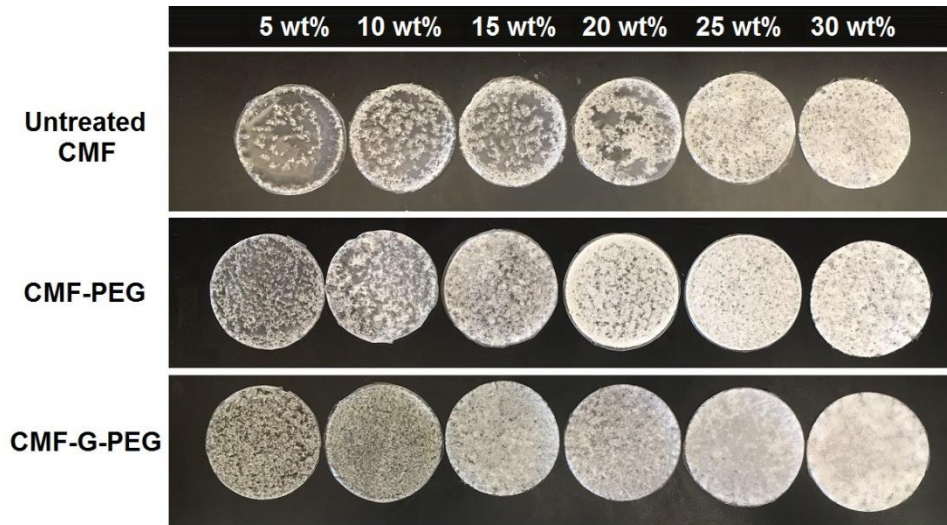


**Fig. 4.** Images of PLA-based biocomposites incorporated with untreated and modified CMFs

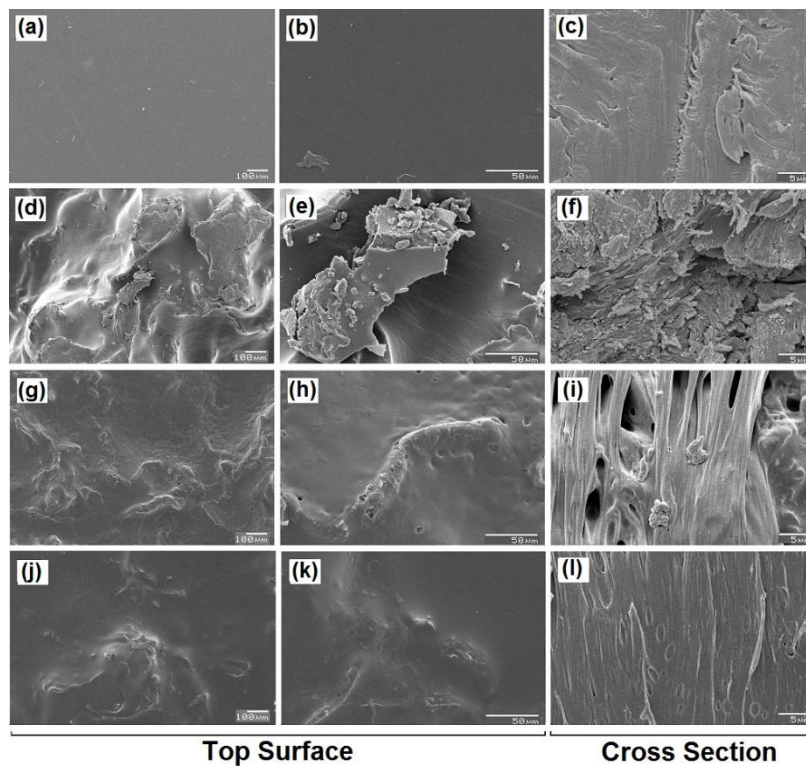


**Fig. 5.** SEM images of: (a, b, and c) neat PLA, (d, e, and f) PLA/C10, (g, h, and i) PLA/CP10, (j, k, and l) PLA/CGP10

Figures 5g-i present the morphology of PLA/CP10. The results illustrate proper dispersion of modified CMF (CMF-PEG) in the PLA matrix, indicating the compatibilizing effect of PEG. These observations are in good agreement with the results reported by Singh *et al.* (2020) that showed PEO improved the dispersibility of cellulose fibers in PLA. The SEM images of PLA/CGP10 are provided in Figs. 5j-l. The results indicate a uniform phase morphology of materials that CMF-G-PEG was homogeneously dispersed in the PLA matrix. Because PEG and PLA are miscible with each other, no phase separation occurred in the PLA/PEG blends at different weight ratios (Sheth *et al.* 1997; Mohapatra *et al.* 2014). Therefore, grafting PEG chains on the surface of fibers can represent an effective modification method for fabricating homogenous PLA/cellulose fibers composites.

The FT-IR analysis was used to study the chemical structure of PLA-based biocomposites, and the results are given in Fig. 6. The spectrum of the neat PLA exhibited the absorption bands of  $\nu_{\text{as}}\text{CH}_3$  at  $2999\text{ cm}^{-1}$ ,  $\nu_{\text{s}}\text{CH}_3$  at  $2950\text{ cm}^{-1}$ ,  $\nu\text{C}=\text{O}$  at  $1753\text{ cm}^{-1}$ ,  $\delta_{\text{as}}\text{CH}_3$  at  $1457\text{ cm}^{-1}$ ,  $\delta_{\text{l}}\text{CH}$  at  $1360\text{ cm}^{-1}$ ,  $\nu\text{COC}$  at  $1259\text{ cm}^{-1}$ ,  $\nu_{\text{as}}\text{CH}_3$  at  $1180\text{ cm}^{-1}$ ,  $\nu_{\text{as}}\text{CH}_3$  at  $1118\text{ cm}^{-1}$ ,  $\nu_{\text{s}}\text{COC}$  at  $1087\text{ cm}^{-1}$ ,  $\nu\text{C}-\text{CH}_3$  at  $1049\text{ cm}^{-1}$ , and  $\nu\text{C}-\text{COO}$  at  $869\text{ cm}^{-1}$ . No major differences can be observed between the neat PLA and PLA/C10. The results suggest poor interfacial adhesion between PLA and untreated fibers, which is in good agreement with the obtained SEM result of PLA/C10 sample.

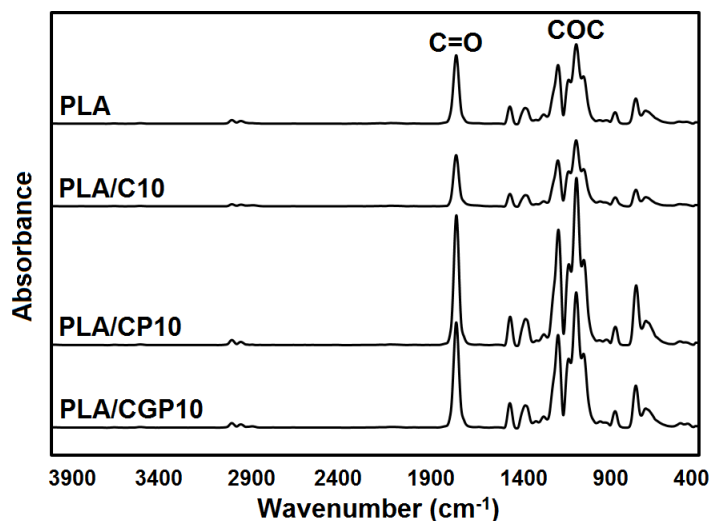


**Fig. 6.** FT-IR spectra of the neat PLA and PLA-based biocomposites

According to the spectra of biocomposites incorporated with modified CMFs, the results displayed that the C=O absorption band of PLA shifted to the lower wavenumbers at  $1749$  and  $1746\text{ cm}^{-1}$  in PLA/CP10 and PLA/CGP10, respectively. Moreover, the intensity of the COC absorption band was remarkably enhanced by the addition of modified CMFs to PLA. It can be deduced that the interaction between PLA and modified CMFs were improved. Possibly owing to the compatibilizing effect of PEG, chemical interactions such as hydrogen bonding can be formed between the terminal hydroxyl and carbonyl groups of PLA and the hydroxyl groups of cellulose (Karimi *et al.* 2019).

The interfacial adhesion between the fiber and polymer is one of the most significant factors influencing the properties of fiber-reinforced composites. Moreover, poor dispersion of fiber in the matrix leads to the formation of voids that can negatively affect the thermomechanical properties and lifespan of materials (Charmi *et al.* 2019). The

results of SEM and FTIR analyses indicate that the modification of CMF with PEG resulted in the improved dispersion of fibers and their interaction with PLA, thereby reducing the void formation and deterioration of mechanical-physical properties of PLA-based composites.

The TGA test was performed to study the thermal stability of PLA-based biocomposites, and the TGA curves are presented in Figs. 7a-c.

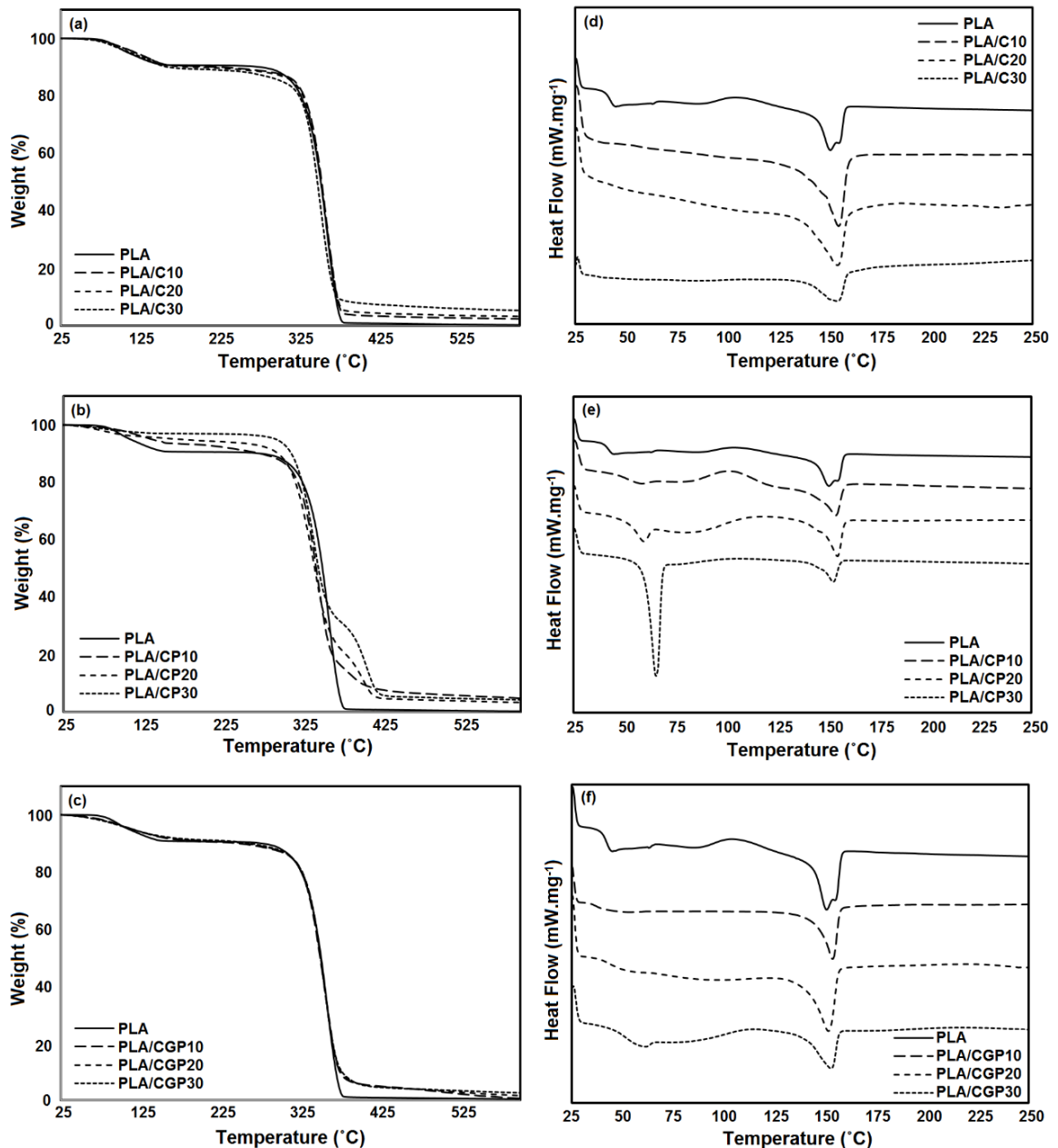


**Fig. 7.** The thermal degradation curves (a, b, and c) and first heating DSC scans (d, e, and f) of the neat PLA and PLA-based biocomposites

The characteristic temperatures of samples, including  $T_{10}$ ,  $T_{max}$ , and  $T_{95}$ , are detailed in Table 3. Overall, the thermal degradation of PLA-based biocomposites occurred between 320 and 420 °C. As mentioned previously, the initial mass loss at temperatures below 200 °C was due to presence of moisture in the samples. The neat PLA showed a single thermal degradation step with a  $T_{max}$  value of 349.23 °C. In TGA results of PLA/C samples, it can be observed that the addition of untreated CMF reduced the onset thermal degradation temperatures ( $T_{10}$ ). However, the end set temperatures ( $T_{95}$ ) shifted towards higher values, indicating the reinforcement effect of cellulose fibers (Johari *et al.* 2016).

The TGA results corresponding to PLA/CP biocomposites exhibit that incorporating CMF-PEG into PLA increased the temperature at the early ( $T_{10}$ ) and final ( $T_{95}$ ) stages of thermal degradation. In the PLA/CGP biocomposites, no remarkable differences were found between the neat PLA and PLA/CGP regarding the onset and maximum thermal decomposition temperatures ( $T_{10}$  and  $T_{max}$ ). However, the end set temperature ( $T_{95}$ ) values remarkably increased with the incorporation of CMF-G-PEG to PLA. It can be concluded that the modified CMFs might act as heat sinks in the PLA matrix that can extract more heat than the polymer, eventually leading to the protection of PLA chains from thermal decomposition (Thongpina *et al.* 2017). A similar result was reported for the PLA/graphene nanocomposite (Botta *et al.* 2018).

The TGA results suggest the modification of cellulose fibers with PEG (having a higher thermal degradation temperature than the PLA matrix), indicating enhanced thermal stability of PLA-based biocomposites in the high-temperature range. Therefore, the prepared membranes could play a key role in improving the safety performance of a building envelope system by increasing the activation energy level required for the thermal decomposition of materials (Abdul-Latif *et al.* 2020).

The DSC analysis was used to determine the thermal properties of PLA-based biocomposites. The first heating DSC curves of samples in a temperature range from 30 to 250 °C are provided in Figs. 7d-f. The neat PLA exhibited the glass transition at 67.91 °C and two melting peaks at 150.62 °C ( $T_{m1}$ ) and 153.98 °C ( $T_{m2}$ ). The double melting peak of PLA is attributed to the melt recrystallization mechanism that has been previously reported in several research studies (Chomachayi *et al.* 2020; Beltrán *et al.* 2021). As shown in Table 3, by incorporating 10 wt% untreated CMF into PLA, the  $T_m$  was enhanced to 154.7 °C and remained unchanged at this value by increasing the CMF content. Moreover, the  $T_g$  of PLA occurred at lower values in PLA/C samples. For instance, after the addition of 10 and 20 wt% of untreated CMF, the  $T_g$  of PLA was reduced to 57.7 °C and 56.1 °C, respectively. It can be assumed that the presence of moisture in fibers leads to the degradation of PLA chains, resulting in the lower values of  $T_g$  (Paunonen *et al.* 2020).

It should be noted that due to the overlap between the glass transition of PLA and the melting peak of PEG, it was difficult to determine the  $T_g$  values of PLA in samples containing modified fibers with PEG. The results in Table 3 indicate that the  $T_m$  values of PLA in PLA/CP and PLA/CGP biocomposites were somewhat higher than that of the neat PLA. The  $T_m$  values of PLA in samples incorporated with 10 wt% of CMF-PEG and CMF-G-PEG were 153.9 °C and 153.5 °C, respectively. This could be due to the decreasing of polymer segmental motions as a result of the improved interfacial adhesion between PLA and modified fibers (Singh *et al.* 2020; Chomachayi *et al.* 2021).

The thermomechanical properties of PLA-based biocomposites were determined by DMA analysis, and the curves of storage modulus ( $E'$ ) and  $\tan \delta$  versus temperature ( $T$ ) are presented in Fig. 8. Moreover, the  $E'$  values at 30 °C and the  $T_g$  of PLA in samples are detailed in Table 3. The abrupt changes in the storage modulus versus temperature curves

of samples from 60 to 75 °C are assigned to the glass transition of PLA. As can be observed in Fig. 8, the addition of untreated and modified CMFs to PLA remarkably reduced the  $E'$  values of PLA-based biocomposites. The results might be attributed to the fibers' agglomeration and formation of voids between the polymer matrix and fibers, thereby diminishing the mechanical properties of materials (Kuan *et al.* 2021; Alasfar *et al.* 2022).

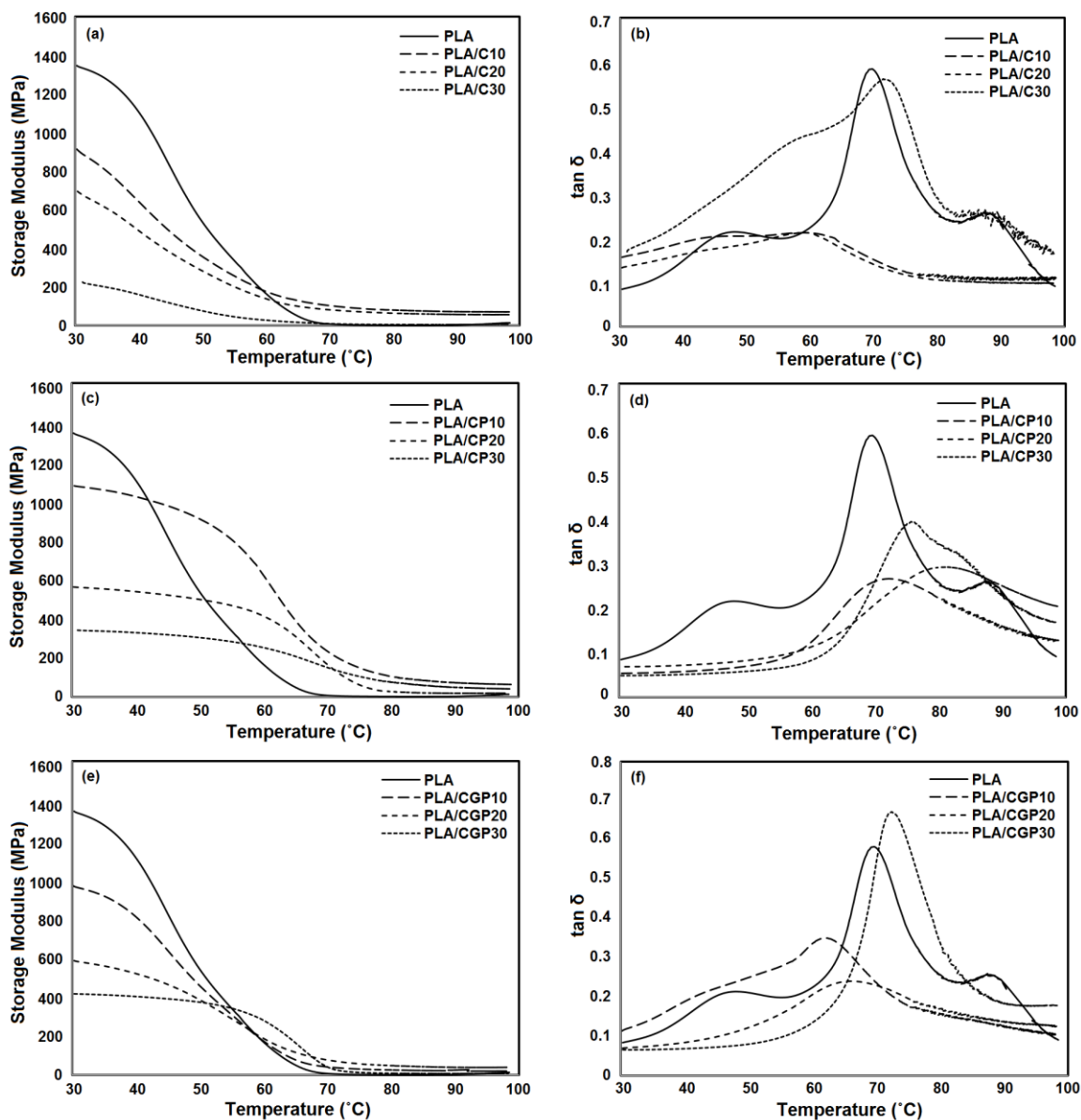


**Fig. 8.** (a, c, and e) DMA storage modulus and (b, d, and f) DMA loss tangent ( $\tan \delta$ ) of the neat PLA and PLA-based biocomposites

The neat PLA exhibited the  $T_g$  at 69.6 °C, which is somewhat higher than the obtained  $T_g$  value from DSC (67.9 °C). According to Table 3, after the addition of 10 and 20 wt% of untreated fibers to PLA, the  $T_g$  values decreased to 59.3 and 59.1 °C, respectively. The observations are in good agreement with the results obtained from the DSC analysis. The  $T_g$  of PLA in PLA/CP biocomposites was remarkably enhanced for all

CMF-PEG contents (10, 20, and 30 wt%). Additionally, the  $T_g$  value of PLA in PLA/CGP biocomposites containing 30 wt% of CMF-G-PEG was 72.5 °C, which is higher than that of neat PLA. It can be concluded that the polymer chains' mobility was restricted owing to the compatibilizing effect of PEG and improvement of the interaction between PLA and cellulose fibers, and consequently, the  $T_g$  value was shifted to higher temperatures (Fortunati *et al.* 2013; Singh *et al.* 2020).

**Table 3.** Thermomechanical Parameters of PLA-based Biocomposites from TGA, DSC, and DMA

Material	$T_{10}$ (°C)	$T_{max}$ (°C)	$T_{95}$ (°C)	$^1T_g$ (PLA) (°C)	$T_m$ (PEG) (°C)	$\Delta H_m$ (PEG) (J.g <sup>-1</sup> )	$T_m$ (PLA) (°C)	$\Delta H_m$ (PLA) (J.g <sup>-1</sup> )	$E'$ (MPa)	$^2T_g$ (PLA) (°C)
PLA	274.78	349.23	372.84	67.91	-	-	150.62	24.42	1345.99	69.60
PLA/C10	222.08	353.28	376.31	57.69	-	-	154.68	31.18	914.99	59.30
PLA/C20	192.49	352.33	387.15	56.08	-	-	154.01	27.61	695.82	59.11
PLA/C30	159.46	347.46	599.23	61.47	-	-	154.08	20.24	226.18	71.28
PLA/CP10	172.36	343.31	420.70	-	57.74	3.69	153.93	21.68	1075.84	72.25
PLA/CP20	272.72	338.62	486.23	-	59.54	7.39	154.93	12.89	558.99	81.03
PLA/CP30	311.76	343.86	584.71	-	65.65	38.43	152.66	9.74	339.53	75.83
PLA/CGP10	199.05	349.06	363.51	-	46.95	3.45	153.50	21.99	964.94	61.84
PLA/CGP20	243.82	349.73	406.13	-	52.24	0.91	151.43	18.48	583.89	66.14
PLA/CGP30	260.01	349.89	416.76	-	58.92	4.08	152.52	18.78	414.44	72.48

<sup>1</sup> $T_{g(PLA)}$  obtained from DSC and <sup>2</sup> $T_{g(PLA)}$  obtained from DMA

The mechanical properties of PLA-based biocomposites were determined by the uniaxial tensile test, and the stress-strain curve and characteristic mechanical properties are provided in Fig. 9. The neat PLA showed 37.5% elongation at break, indicating that the particular grade of PLA (4043D) is appropriate for the fabrication of bio-based membranes. The incorporation of untreated CMF into PLA extensively decreased the tensile strength and Young's modulus values of materials. In addition, the elongation at break remarkably reduced as the bio-fillers content increased, indicating the compromise of the flexibility of materials. For instance, by adding 30 wt% of CMF to PLA, the elongation at break values decreased from 37.5% to 3.44%. This might be attributed to the agglomeration of untreated fibers in the PLA matrix and the lack of affinity between PLA and CMF (Lu *et al.* 2014; Balali *et al.* 2018; Singh *et al.* 2020).

The PLA/CP samples showed no improvement in mechanical performance compared to PLA/C. However, the PLA/CGP10 sample (PLA containing 10 wt% of CMF-G-PEG) exhibited the highest value of elongation at break (6.77%) among all biocomposites. This could be attributed to the plasticizing and compatibilizing effect of PEG on PLA/cellulose fibers composites (Li *et al.* 2018).

Ideally, membranes used in building envelope systems should have excellent mechanical characteristics in terms of elongation and tear resistance. In the other words, the membrane should be flexible and foldable enough to take any shape it is laid over and be able to cover walls and move with the building (Balali *et al.* 2018). The mechanical investigation showed that the flexibility of PLA-based biocomposites was improved by grafting PEG onto the surface of cellulose fibers, and PLA/CGP10 sample having the highest value of flexibility could be considered a suitable candidate for the fabrication of membranes for building envelope applications.

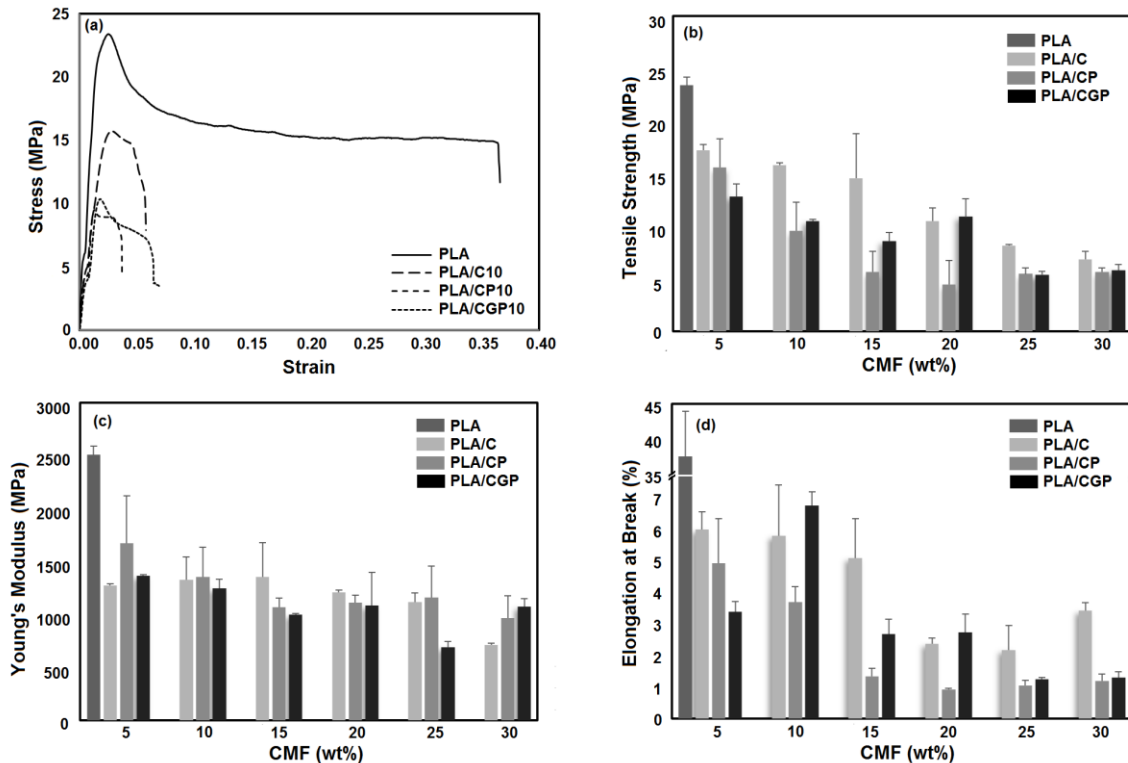


**Fig. 9.** Stress-strain curve and tensile results of the neat PLA and PLA-based biocomposites

The water vapor permeability is one of the critical properties of materials in several applications, including building envelopes. The transmission of water vapor through building materials takes place due to: (1) vapor pressure gradient from one side of materials to the other, (2) the area of materials, and (3) the permeance properties of materials. Several parameters can affect the permeability properties of polymers, such as degree of crystallinity, porosity, hydrophobicity/hydrophilicity of materials, the segmental orientation of polymer chains, and the addition of micro/nano fillers to the polymeric matrix (Bouakaz *et al.* 2017; Chomachayi *et al.* 2020). The water vapor transmission rate (WVTR) of PLA-based biocomposites was examined, and the results are provided in Fig. 10. Moreover, the values of WVTR, normalized WVTR, and water vapor permeability ( $P$ ) are detailed in Table 4. The results indicate that the addition of untreated cellulose fibers noticeably increased the  $P$ -values of materials. As mentioned before, cellulose fibers have hydrophilic characteristics and large amounts of hydroxyl groups that enhance the hydrophilicity of materials. Hence, their presence in biocomposites can ease moisture diffusion from the surroundings. Moreover, the agglomeration of CMF in PLA and the formation of voids between the polymer matrix and fibers can create a preferential pathway for the transport of water vapor molecules in materials. Hussain and Blanchet (2021) previously demonstrated that the values of water vapor transmission increased by incorporating cellulose fibers into the PLA matrix.

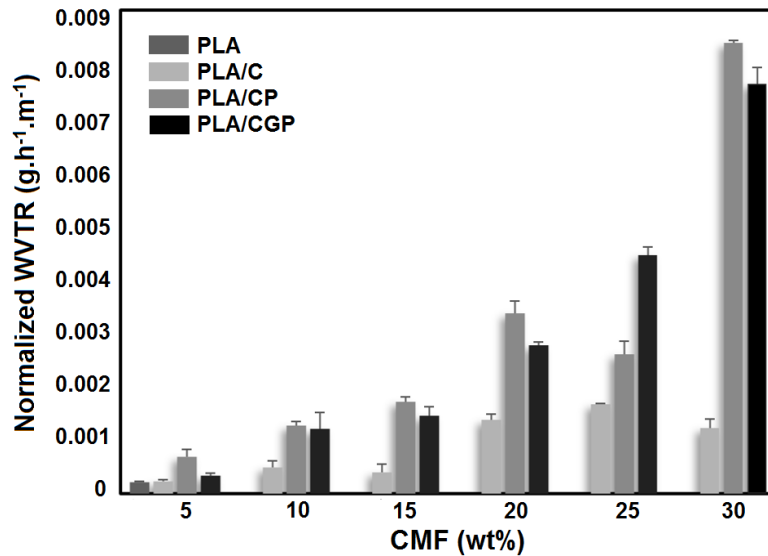


Fig. 10. The normalized WVTR values of the neat PLA and PLA-based biocomposites

Table 4. The WVTR, Normalized WVTR, and Permeability Values of Neat PLA and PLA-based Biocomposites

Material	WVTR (g.h <sup>-1</sup> .m <sup>-2</sup> )	Normalized WVTR (g.h <sup>-1</sup> .m <sup>-1</sup> ) × 10 <sup>-5</sup>	Permeability (g.h <sup>-1</sup> .m <sup>-1</sup> .Pa <sup>-1</sup> ) × 10 <sup>-7</sup>
PLA	1.4 ± 0.1	21.3 ± 2.7	1.4 ± 0.2
PLA/C5	0.7 ± 0.1	23.1 ± 3.4	1.6 ± 0.2
PLA/C10	1.1 ± 0.3	49.3 ± 12.8	3.5 ± 0.9
PLA/C15	1.1 ± 0.4	3.4 ± 15.8	2.8 ± 1.1
PLA/C20	2.9 ± 0.2	137.9 ± 9.9	9.8 ± 0.7
PLA/C25	2.5 ± 0.1	166.2 ± 2.8	11.8 ± 0.2
PLA/C30	2.4 ± 0.3	121.9 ± 17.3	8.7 ± 1.2
PLA/CP5	1.9 ± 0.1	69.6 ± 12.4	4.9 ± 0.9
PLA/CP10	2.5 ± 0.1	127.1 ± 7.2	9.1 ± 0.5
PLA/CP15	3.2 ± 0.3	171.7 ± 8.1	12.2 ± 0.6
PLA/CP20	6.7 ± 0.5	336.7 ± 22.6	23.9 ± 1.6
PLA/CP25	5.9 ± 0.3	259.9 ± 23.7	18.5 ± 1.7
PLA/CP30	13.1 ± 0.1	839.2 ± 5.1	59.7 ± 0.4
PLA/CGP5	1.2 ± 0.1	34.1 ± 4.7	2.4 ± 0.3
PLA/CGP10	2.7 ± 0.5	120.4 ± 30.5	8.6 ± 2.1
PLA/CGP15	2.9 ± 0.3	145.5 ± 16.3	10.3 ± 1.1
PLA/CGP20	5.2 ± 0.1	276.5 ± 5.9	19.7 ± 0.4
PLA/CGP25	6.1 ± 0.2	443.6 ± 16.5	31.6 ± 1.2
PLA/CGP30	10.6 ± 0.4	762.6 ± 31.3	54.2 ± 2.2

Concerning the effect of fiber modification on the permeability, the results indicate that the PLA/CP and PLA/CGP samples showed higher values of P compared to the PLA/C. For instance, the normalized WVTR value of PLA incorporated with 20 wt% of untreated CMF (PLA/C20) was about 143% and 100% lower than that of PLA/CP20 and PLA/CGP20, respectively. It is worth noting that PEG is a hydrophilic biopolymer, and because of its terminal hydroxyl end groups, it has a high solubility in water (Chen *et al.* 2014). Therefore, it could be deduced that the modification with PEG imposes more hydrophilic characteristics on cellulose fibers. Consequently, the water vapor transmission

through the sample films is enhanced with the addition of modified fibers. Additionally, the *P*-values of PLA/CGP were somewhat lower than PLA/CP samples (except for the 25 wt% of modified CMFs). The results could be attributed to the better dispersion of CMF-G-PEG in the PLA matrix that reduced the formation of voids in composites necessary for the capillary movement of water vapor molecules (Chomachayi *et al.* 2020; Beltrán *et al.* 2021).

The incorporation of modified CMFs to PLA can regulate humidity by facilitating the transmission of water vapor from the interior atmosphere of building to the outside. Therefore, the developed membrane with enhanced permeability properties could prevent the mold growth, moisture build-up, and dampening of building envelopes which would otherwise lead to economic damage and impair the building's indoor air quality (Eder and Carus 2013; Alasfar *et al.* 2022).

## CONCLUSIONS

1. This study aimed to develop bio-based polymeric membranes for building envelope applications. In this regard, PLA-based biocomposites containing up to 30 wt% of natural cellulose microfibrils (CMF) were successfully produced by the solvent casting method. To improve the interfacial adhesion between the bio filler and biopolymer matrix, CMF was modified using two methods: Mixing CMF with PEG (CMF-PEG) and grafting PEG onto CMF (CMF-G-PEG).
2. The morphology results indicated that both modification methods remarkably increased the dispersibility of cellulose fibers in the PLA matrix.
3. The incorporation of modified CMFs into PLA enhanced the glass transition temperature and final thermal decomposition temperature of materials.
4. The values of water vapor permeability of PLA-based biocomposites enhanced as the modified CMFs content increased in the materials.
5. The results of the tensile analysis demonstrated that simply mixing CMF with PEG is not sufficient to provide the desired mechanical properties. However, PLA incorporated with 10 wt% of CMF-G-PEG showed the highest elongation at break value among all PLA-based biocomposites.
6. The resulting PLA-based membranes with enhanced permeability performance exhibit considerable potential in the construction industry by improving indoor air quality as well as reducing the deterioration of building materials. The approach used in this research work for the fabrication of green biocomposites incorporated with both cellulose microfibrils and PEG could pave the way to produce sustainable thermoplastic biocomposites with high loadings of cellulose microfibrils that could have a wide range of applications in several sectors of the plastic industry. Future work is recommended considering the hydrophobic treatment of cellulose microfibrils and the solvent-free extrusion process for the fabrication of PLA/CMF composites as well as the examination of their weathering and durability performance.

## ACKNOWLEDGMENTS

The authors are thankful to Natural Sciences and Engineering Research Council (NSERC) of Canada for the financial support through its IRC and CRD programs (IRCPJ 461745-18 and RDCPJ 524504-18) as well as the industrial partner, Kruger Inc., of the NSERC industrial chair on eco-responsible wood construction (CIRCERB).

## Conflict of Interest

The authors declare that there is no conflict of interest. The funders had no role in the design of the study; in the collection, analyses, and interpretation of data; in the writing of the manuscript, and in the decision to publish the results.

## REFERENCES CITED

- Abdul-Latif, N.-I. S., Ong, M. Y., Nomanbhay, S., Salman, B., and Show, P. L. (2020). "Estimation of carbon dioxide (CO<sub>2</sub>) reduction by utilization of algal biomass bioplastic in Malaysia using carbon emission pinch analysis (CEPA)," *Bioengineered* 11(1), 154-164. DOI: 10.1080/21655979.2020.1718471
- Alasfar, R. H., Ahzi, S., Barth, N., Kochkodan, V., Khraisheh, M., and Koç, M. (2022). "A review on the modeling of the elastic modulus and yield stress of polymers and polymer nanocomposites: Effect of temperature, loading rate and porosity," *Polymers* 14(3), 360. DOI: 10.3390/polym14030360
- Arregi, B., Garay-Martinez, R., Astudillo, J., Garcia, M., and Ramos, J. C. (2020). "Experimental and numerical thermal performance assessment of a multi-layer building envelope component made of biocomposite materials," *Energy Build* 214, article no. 109846. DOI: 10.1016/j.enbuild.2020.109846
- Astudillo, J., Garcia González, M., Sacristán, J., Uranga, N., Leivo, M., Mueller, M., Roig, I., Langer, S., Gemignani, G., and Vilkki, M. (2018). "New biocomposites for innovative construction façades and interior partitions," *J. Facade Des. Eng* 6(2), 65-83. DOI: 10.7480/jfde.2018.2.2104
- ASTM D882-10 (2010). "Standard test method for tensile properties of thin plastic sheeting," ASTM International, West Conshohocken, USA.
- ASTM standard E 96/E96M-16 (Method B) (2016). "Standard test methods for water vapor transmission of materials," ASTM International, West Conshohocken, USA.
- Balali, S., Davachi, S. M., Sahraeian, R., Shiroud Heidari, B., Seyfi, J., and Hejazi, I. (2018). "Preparation and characterization of composite blends based on polylactic acid/polycaprolactone and silk," *Biomacromolecules* 19(11), 4358-4369. DOI: 10.1021/acs.biomac.8b01254
- Beltrán, F. R., Gaspar, G., Chomachayi, M. D., Jalali-Arani, A., Lozano-Pérez, A. A., Cenis, J. L., Maria, U., Pérez, E., and Urreaga, J. M. M. (2021). "Influence of addition of organic fillers on the properties of mechanically recycled PLA," *Environ. Sci. Pollut. Res* 28(19), 24291-24304. DOI: 10.1007/s11356-020-08025-7
- Bledzki, A. K., and Gassan, J. (1999). "Composites reinforced with cellulose based fibres," *Prog. Polym. Sci* 24(2), 221-274. DOI: 10.1016/S0079-6700(98)00018-5
- Botta, L., Scaffaro, R., Suter, F., and Mistretta, M. C. (2018). "Reprocessing of PLA/graphene nanoplatelets nanocomposites," *Polymers* 10(1), 18. DOI: 10.3390/polym10010018

- Bouakaz, B. S., Habi, A., Grohens, Y., and Pillin, I. (2017). "Organomontmorillonite/graphene-PLA/PCL nanofilled blends: New strategy to enhance the functional properties of PLA/PCL blend," *Appl. Clay Sci* 139, 81-91. DOI: 10.1016/j.clay.2017.01.014
- Charmi, J., Nosrati, H., Amjad, J. M., Mohammadkhani, R., and Danafar, H. (2019). "Polyethylene glycol (PEG) decorated graphene oxide nanosheets for controlled release curcumin delivery," *Heliyon* 5(4), 01466. DOI: 10.1016/j.heliyon.2019.e01466
- Chen, M., Wang, W., and Wu, X. (2014). "One-pot green synthesis of water-soluble carbon nanodots with multicolor photoluminescence from polyethylene glycol," *J. Mater. Chem. B* 2(25), 3937-3945. DOI: 10.1039/C4TB00292J
- Chomachayi, M. D., Jalali-arani, A., Beltrán, F. R., de la Orden, M. U., and Urreaga, J. M. (2020). "Biodegradable nanocomposites developed from PLA/PCL blends and silk fibroin nanoparticles: Study on the microstructure, thermal behavior, crystallinity and performance," *J. Polym. Environ* 28, 1252-1264. DOI: 10.1007/s10924-020-01684-0
- Dadras Chomachayi, M., Jalali-arani, A., and Martínez Urreaga, J. (2021). "A comparison of the effect of silk fibroin nanoparticles and microfibers on the reprocessing and biodegradability of PLA/PCL blends," *J. Polym. Environ* 29, 2585-2597. DOI: 10.1007/s10924-021-02053-1
- Eder, A., and Carus, M. (2013). "Global trends in wood-plastic composites (WPC)," *Bioplastics Magazine*, (<http://www.wpc-consulting.eu>).
- Fortunati, E., Puglia, D., Kenny, J. M., Haque, M. M.-U., and Pracella, M. (2013). "Effect of ethylene-co-vinyl acetate-glycidylmethacrylate and cellulose microfibers on the thermal, rheological and biodegradation properties of poly (lactic acid) based systems," *Polym. Degrad. Stab* 98(12), 2742-2751. DOI: 10.1016/j.polymdegradstab.2013.10.007
- Gustavsson, L., and Sathre, R. (2006). "Variability in energy and carbon dioxide balances of wood and concrete building materials," *Build. Environ* 41(7), 940-951. DOI: 10.1016/j.buildenv.2005.04.008
- Hussain, A., and Blanchet, P. (2021). "Preparation of breathable cellulose based polymeric membranes with enhanced water resistance for the building industry," *Materials* 14(15), article no. 4310. DOI: 10.3390/ma14154310
- Iwano, J., and Mwashia, A. (2013). "The impact of sustainable building envelope design on building sustainability using Integrated Performance Model," *Int. J. Sustain. Built. Environ* 2(2), 153-171. DOI: 10.1016/j.ijbsbe.2014.03.002
- Johari, A. P., Kurmvanshi, S. K., Mohanty, S., and Nayak, S. K. (2016). "Influence of surface modified cellulose microfibrils on the improved mechanical properties of poly (lactic acid)," *Int. J. Biol. Macromol* 84, 329-339. DOI: 10.1016/j.ijbiomac.2015.12.038
- Johari, A. P., Mohanty, S., Kurmvanshi, S. K., and Nayak, S. K. (2016). "Influence of different treated cellulose fibers on the mechanical and thermal properties of poly (lactic acid)," *ACS Sustain. Chem. Eng* 4(3), 1619-1629. DOI: 10.1021/acssuschemeng.5b01563
- Karimi, S., Ghasemi, I., and Abbassi-Sourki, F. (2019). "A study on the crystallization kinetics of PLLA in the presence of graphene oxide and PEG-grafted-graphene oxide: Effects on the nucleation and chain mobility," *Compos. B. Eng* 158, 302-310. DOI: 10.1016/j.compositesb.2018.10.004

- Kuan, H. T. N., Tan, M. Y., Shen, Y., and Yahya, M. Y. (2021). "Mechanical properties of particulate organic natural filler-reinforced polymer composite: A review," *Compos. Adv. Mater* 30, 1-17. DOI: 10.1177/26349833211007502
- Lanzillotto, M., Konnert, L., Lamaty, F., Martinez, J., and Colacino, E. (2015). "Mechanochemical 1,1'-carbonyldiimidazole-mediated synthesis of carbamates," *ACS Sustain. Chem. Eng* 3(11), 2882-2889. DOI: 10.1021/acssuschemeng.5b00819
- Li, D., Jiang, Y., Lv, S., Liu, X., Gu, J., Chen, Q., and Zhang, Y. (2018). "Preparation of plasticized poly (lactic acid) and its influence on the properties of composite materials," *PLoS One* 13(3), article no. 193520. DOI: 10.1371/journal.pone.0193520
- de Lima, G. F., de Souza, A. G., and Rosa, D. S. (2018). "Effect of adsorption of polyethylene glycol (PEG), in aqueous media, to improve cellulose nanostructures stability," *J. Mol. Liq* 268, 415-424. DOI: 10.1016/j.molliq.2018.07.080
- Lu, T., Liu, S., Jiang, M., Xu, X., Wang, Y., Wang, Z., Gou, J., Hui, D., and Zhou, Z. (2014). "Effects of modifications of bamboo cellulose fibers on the improved mechanical properties of cellulose reinforced poly (lactic acid) composites," *Compos. B. Eng* 62, 191-197. DOI: 10.1016/j.compositesb.2014.02.030
- Mármol, G., Gauss, C., and Fangueiro, R. (2020). "Potential of cellulose microfibrils for PHA and PLA biopolymers reinforcement," *Molecules* 25(20), article no. 4653. DOI: 10.3390/molecules25204653
- Mohapatra, A. K., Mohanty, S., and Nayak, S. K. (2014). "Effect of PEG on PLA/PEG blend and its nanocomposites: A study of thermo-mechanical and morphological characterization," *Polym. Compos* 35(2), 283-293. DOI: 10.1002/pc.22660
- Paunonen, S., Berthold, F., and Immonen, K. (2020). "Poly(lactic acid)/pulp fiber composites: The effect of fiber surface modification and hydrothermal aging on viscoelastic and strength properties," *J. Appl. Polym. Sci* 137(42), article no. 49617. DOI: 10.1002/app.49617
- Sheth, M., Kumar, R. A., Davé, V., Gross, R. A., and McCarthy, S. P. (1997). "Biodegradable polymer blends of poly (lactic acid) and poly (ethylene glycol)," *J. Appl. Polym. Sci* 66(8), 1495-1505. DOI: 10.1002/(SICI)1097-4628(19971121)66:8<1495::AID-APP10>3.0.CO;2-3
- Singh, A. A., Genovese, M. E., Mancini, G., Marini, L., and Athanassiou, A. (2020). "Green processing route for polylactic acid-cellulose fiber biocomposites," *ACS Sustain. Chem. Eng* 8(10), 4128-4136. DOI: 10.1021/acssuschemeng.9b06760
- Zeng, Q., Wang, Y., Wang, Y., Cao, W., Liu, C., and Shen, C. (2019). "Polyethylene oxide-assisted dispersion of graphene nanoplatelets in poly(lactic acid) with enhanced mechanical properties and crystallization ability," *Polym. Test* 78, article no. 106008. DOI: 10.1016/j.polymertesting.2019.106008
- Ye, A., Wang, S., Zhao, Q., Wang, Y., Liu, C., and Shen, C. (2019). "Poly(ethylene oxide)-promoted dispersion of graphene nanoplatelets and its effect on the properties of poly (lactic acid)/poly (butylene adipate-co-terephthalate) based nanocomposites," *Mater. Lett* 253, 34-37. DOI: 10.1016/j.matlet.2019.06.040
- Siró, I., and Plackett, D. (2010). "Microfibrillated cellulose and new nanocomposite materials: a review," *Cellulose* 17(3), 459-494. DOI: 10.1007/s10570-010-9405-y
- Thongpina, C., Tippuwanan, C., Buaksuntear, K., and Chuawittayawuta, T. (2017). "Mechanical and thermal properties of PLA melt blended with high molecular weight PEG modified with peroxide and organo-clay," *Key Eng. Mater* 751, 337-343. DOI: 10.4028/www.scientific.net/KEM.751.337

Yazdani, M. R., Ajdary, R., Kankkunen, A., Rojas, O. J., and Seppälä, A. (2021).  
“Cellulose nanofibrils endow phase-change polyethylene glycol with form control  
and solid-to-gel transition for thermal energy storage,” *ACS Appl. Mater. Interfaces*  
13(5), 6188-6200. DOI: 10.1021/acsami.0c18623

Article submitted: June 28, 2022; Peer review completed: August 6, 2022; Revised  
version received and accepted: August 9, 2022; Published: August 12, 2022.  
DOI: 10.15376/biores.17.4.5707-5727